Modulation analysis of large-scale discrete vortices

Modulation analysis of large-scale discrete vortices

Luis A. Cisneros,[1,*] Antonmaria A. Minzoni,[2,†] Panayotis Panayotaros,[2,‡] and Noel F. Smyth[3,§]
[1]*Department of Mathematics and Statistics, University of New Mexico, Albuquerque, New Mexico 87131-0001, USA*
[2]*Fenomenos Nonlineales y Mecánica (FENOMEC), Department of Mathematics and Mechanics, Instituto de Investigación en Matemáticas Aplicadas y Sistemas, Universidad Nacional Autónoma de México, 01000 México Distrito Federal, Mexico*
[3]*School of Mathematics and Maxwell Institute for Mathematical Sciences, The King's Buildings, University of Edinburgh, Edinburgh EH9 3JZ, United Kingdom*
(Received 13 May 2008; published 17 September 2008)

The behavior of large-scale vortices governed by the discrete nonlinear Schrödinger equation is studied. Using a discrete version of modulation theory, it is shown how vortices are trapped and stabilized by the self-consistent Peierls-Nabarro potential that they generate in the lattice. Large-scale circular and polygonal vortices are studied away from the anticontinuum limit, which is the limit considered in previous studies. In addition numerical studies are performed on large-scale, straight structures, and it is found that they are stabilized by a nonconstant mean level produced by standing waves generated at the ends of the structure. Finally, numerical evidence is produced for long-lived, localized, quasiperiodic structures.

DOI: 10.1103/PhysRevE.78.036604 PACS number(s): 05.45.Yv, 42.65.Tg

I. INTRODUCTION

The discrete nonlinear Schrödinger (DNLS) equation is a nonlinear lattice model that appears in many areas of science and which has attracted a lot of attention in recent years. One such area is nonlinear optics, where the usefulness of the DNLS equation as a model for coherent light propagation in waveguide arrays has been well established [1–4]. The DNLS equation has also been used to describe Bose-Einstein condensates in optical lattices [5], as well as energy transfer in biomolecular chains [6,7].

A major effect of a nonlinear lattice is the localization of energy in a few "active" sites. This was first noted by Sievers and Takeno [8]. Subsequent theoretical studies have explained localization by showing the existence of breather solutions, defined as spatially decaying time-periodic solutions for which each site has the same temporal frequency [9–12]. The existence of these stable (and unstable) breathers in one- and higher-spatial-dimensional lattices is well understood. In the case of breathers near the limit of vanishing site coupling, the "anticontinuous limit" [9], the set of active sites can be an arbitrary finite subset of the integer lattice. Breathers are also robust in that they appear in several variants of the DNLS equation [13,15,14] and in other lattice models. Breathers with two quasiperiods in time have also been shown to exist [16].

In the present work we examine localized structures from a different perspective, with emphasis on the spatial features of the localized structure and leaving the temporal behavior undetermined *a priori*. This allows us to understand theoretically the dynamical behavior of localized structures that are difficult to analyze using the breather ansatz. Moreover, we allow structures that have a more general temporal behavior. The first these solutions examined are vortexlike solutions, which are discrete analogs of the circular vortex solutions of the continuous NLS equation. In the limit of large radius and small width to radius ratio, an asymptotic theory based on a modulated vortex ansatz in an averaged Lagrangian predicts the existence of stable and unstable localized solutions with suitable width to radius ratios. These structures are also found numerically and their stability properties coincide with the theoretical predictions. Spatiotemporal modulation of these structures corresponds to wavelike modes which propagate in the angular direction around the vortex, with the vortex eventually evolving to a time-periodic localized state. We find furthermore that the discretization effects arising through the Peierls-Nabarro potential can stabilize perturbations which correspond to unstable modes of the continuous NLS vortex. In the wavelike structures we find sizable spatial and temporal variations in the amplitude and phase of the sites, which suggests that we are far from the small-coupling discrete vortex breathers of the type described by Pelinovsky *et al.* [12].

The second type of solution we examine is localized in thin parallelogram sets. We assume that the width to length ratio of the parallelogram is small and use an averaged Lagrangian with a suitable ansatz to find periodic, spatially localized solutions. We find again basic stable states and wavelike structures that move along the length of the parallelogram, bouncing from the two ends. In this parallelogram case, however, the modulation does not decay, suggesting either much slower radiation of these modes, or a new stable state with a standing wave that cannot be captured by the breather ansatz.

Additionally we study numerically localization along polygons whose sides are thin parallelograms. The behavior is qualitatively similar to that seen in the circular vortex case, in that we see stable localization with some modulation. In another set of numerical experiments we examine localization on smaller sets, analyzing the evolution of each site in more detail. We see sites that evolve in an approximately periodic manner, but with periods that are not the same for all sites. These localized states do not show any tendency to

*cisneros@math.unm.edu
†tim@mym.iimas.unam.mx
‡panos@mym.iimas.unam.mx
§N.Smyth@ed.ac.uk

decay and may constitute another type of stable or metastable localized state which is not a breather. Further comments on possible interpretations of the numerical results are given in the Conclusions.

II. FORMULATION AND CIRCULAR VORTICES

Let us consider the two-space-dimensional DNLS equation on the infinite square lattice, labeled by the integers n,m with $-\infty<m,n<\infty$, in the form

$$i\dot{u}_{mn}=\Delta_{mn}u_{mn}+\delta^{-1}|u_{mn}|^2u_{mn}. \tag{1}$$

Here Δ_{mn} is the second-order difference operator in the variables m and n and time derivatives are denoted by an overdot.

In the present work we are interested in finding localized solutions of the DNLS equation (1) with extended, nontrivial shapes, and periodic, and possibly more general, time dependence. It is well known that in the continuum limit $\delta\to\infty$ all pulselike solutions collapse (blow up) and that other localized initial conditions behave in a similar manner. This collapse behavior is due to the focusing nonlinearity. On the other hand, in the so-called anticontinuum limit $\delta\to 0$ the discrete NLS equation (1) has time-periodic solutions of the form

$$u_{mn}=A_{mn}e^{-i\sigma t}e^{i\theta_{mn}}, \tag{2}$$

where, for an arbitrary set of sites m,n, $A_{mn}=A$, $\sigma=A^2/\delta$, and θ_{mn} is arbitrary, while $u_{mn}=0$ for the remaining sites. These solutions are clearly localized around an arbitrary shape. Using bifurcation theory ideas, it was shown by Pelinovsky *et al.* [12] that for small δ these solutions can be continued uniquely (up to a global phase) in δ, provided that the θ_{mn} are chosen appropriately. One then obtains a branch of periodic solutions for which A_{mn} and θ_{mn} depend on δ. This procedure can be used to effectively calculate branches of solutions in cases for which the set of active sites is small or has a simple geometry. For example, in the case of a closed polygonal line shape where each active site has only two active neighbors, solutions can be found for which θ_{mn} increases by an arbitrary integer multiple 2π around a circuit [12]. These "discrete vortices" are examples of breathers [9], since breathers are, by definition, time-periodic solutions for which each site has the same frequency.

Let us now study the behavior of vortex-type solutions that are localized on larger sets and exist for larger δ. We shall also leave the time dependence undetermined and so consider possible solutions that are generalizations of breathers. In order to look at larger vortex-type solutions, we need to capture with a continuum coherent solution both the fact that there is a large number of active sites, and by the Peierls-Nabarro potential the effect of the discrete lattice on this coherent solution. This is achieved using Whitham modulation theory [17] on the averaged Lagrangian for the discrete NLS equation (1),

$$L=\int\sum_{mn}[i(u_{mn}^*\dot{u}_{mn}-u_{mn}\dot{u}_{mn}^*)+\nabla_{mn}u_{mn}\nabla_{mn}u_{mn}^*-\delta^{-1}|u_{mn}|^4]dt. \tag{3}$$

Here the superscript asterisk denotes the complex conjugate and ∇_{mn} is the discrete gradient vector based on forward differences. Appropriate trial functions with time-dependent parameters will be used to represent localized periodic solutions and their evolution (modulations).

Let us begin by studying circular vortices and their stability. The appropriate trial function for this case is

$$u_{mn}=a\sqrt{m^2+n^2}(\operatorname{sech}\psi)e^{i\varphi}+ige^{i\theta_{mn}+i\sigma(t)}, \tag{4}$$

$$\varphi=\theta_{mn}+[\sqrt{m^2+n^2}-R(t)]V(t)+\sigma(t), \tag{5}$$

$$\psi=\frac{\sqrt{m^2+n^2}-R(t)}{w}, \tag{6}$$

$$\theta_{mn}=\tan^{-1}n/m. \tag{7}$$

This trial function represents a vortex of width w concentrated on a circle of radius R, with the phase increasing by 2π around it. The vortex parameters a and w and the shelf height g are assumed to be functions of time t and the polar angle θ. As in previous studies of the stability of nonlocal continuum vortices, it will be assumed that the amplitude a is related, to leading order, to the width w by conservation of mass for the vortex [18]. This assumption is equivalent to a linear stability analysis for the vortex. The shelf, of height g, will be assumed to be concentrated at the peak of the vortex and to have a width Λ_1 which will be determined as part of the analysis [18]. Hence g is nonzero only in the region $r_{\min}<r<r_{\max}$, where $r_{\min,\max}=R\mp\Lambda_1/2$. The phase variable of the vortex ring accounts for its contraction or expansion.

The averaged Lagrangian is determined by substituting the trial function into the Lagrangian. The double sums involved are calculated using Poisson's formula, which gives

$$\sum_{mn}f(m,n)=\sum_{mn}\hat{f}(2\pi m,2\pi n), \tag{8}$$

where $\hat{f}$ denotes the Fourier transform of f, given by

$$\hat{f}(\xi,\eta)=\int_{-\infty}^{\infty}\int_{-\infty}^{\infty}f(x,y)e^{-i(\xi x+\eta y)}dx\,dy. \tag{9}$$

The first term of the series (8) with $m=n=0$ gives the continuum approximation. The rest of the series gives the self-consistent Peierls-Nabarro potential generated by the interaction between the continuum vortex and the lattice. As in other discrete problems [19], to leading order finite differences of u_{mn} are replaced by the equivalent derivatives. Finally, the dominant contributions for the Poisson sum (8) are given by the terms $m=\pm 1$, $n=0$ and $m=0$, $n=\pm 1$. Moreover, for small δ, to leading order, only the δ^{-1} term contributes to the averaged Lagrangian terms which arise from the sum. In this manner, on using polar coordinates to calculate

the continuum contribution, the averaged Lagrangian (3) becomes

$$L = \int_{t_0}^{t_1}\int_0^{2\pi}\int_0^{\infty}\left(ir(u^*u_t - uu_t^*) + r|u_r|^2 + \frac{1}{r}|u_\theta|^2 - \frac{r}{\delta}|u|^4\right)dr\,d\theta\,dt - \int_{t_0}^{t_1}\sum_{|n|=|m|=1}^{\infty}\delta^{-1}\widehat{|u|^4}(2\pi m, 2\pi n)dt = L_0 + L_p. \quad (10)$$

In the integral term of this averaged Lagrangian the trial function (4) is replaced by the continuous function obtained by replacing $\sqrt{m^2+n^2}$ by r and θ_{mn} by the polar angle θ. Since we are assuming that $w \sim \delta \ll 1$, the integrals involved in the averaged Lagrangian (10) are easily calculated. In fact, since $R \gg w$ and the vortex is peaked at $r=R$, the integrals can be reduced to integrals involving sech and its powers and derivatives. Moreover, it is assumed that the shelf has the form $rg(\theta)$. It can then be found that the density $\mathcal{L}_0$ of the averaged Lagrangian is

$$\frac{\mathcal{L}_0}{2\pi} = -(2a^2wR^3 + 4\Lambda_1 R^3 g^2)\dot{\sigma} - 2awR^2 g\dot{w} - 2a^2R^3 w\left(V\dot{R} - \frac{1}{2}V^2\right) - I\frac{a^2R}{w}w_\theta^2 - \frac{2\Lambda_1}{R}g_\theta^2 + 4\delta^{-1}a^2wR^5g^2 - 4a^2wR - \frac{2a^2R^3}{3w} + \frac{2}{3}\delta^{-1}a^4wR^5, \quad (11)$$

where

$$I = \int_{-\infty}^{\infty}\eta^2(\mathrm{sech}^2\,\eta)(\tanh^2\,\eta)d\eta. \quad (12)$$

As in the continuum case [18], small contributions due to terms involving a_θ have been neglected, as these terms are $O(R^{-2})$ compared with the retained terms. The width Λ_1 of the shelf will be determined in the following section.

To calculate the density $\mathcal{L}_p$ the Fourier transform of $|u|^4$ is calculated in polar coordinates. Since R is assumed to be large, the angular integral is calculated using the method of stationary phase. The radial integral is then calculated to leading order by closing the contour in the appropriate half plane, resulting in

$$\mathcal{L}_p = \frac{16\pi^{5/2}}{3\delta}a^4w^4R^{9/2}e^{-\pi^2 w}\cos(2\pi R - \pi/4) = H(R,w). \quad (13)$$

This term of the averaged Lagrangian gives the self-consistent Peierls-Nabarro potential generated by the interaction of the circular vortex and the lattice.

III. MODULATION EQUATIONS AND CIRCULAR VORTICES

Taking variations of the averaged Lagrangian term (11) with respect to σ gives the conservation of mass equation

$$\frac{d}{dt}a^2wR^3 = 0. \quad (14)$$

As in the continuum case [18], this mass conservation equation relates variations in the vortex amplitude and width. The variational equations in V and R give equations for the motion of the vortex as

$$\dot{R} = V \quad (\delta V), \quad (15)$$

$$\frac{d}{dt}(a^2wR^3V) + \frac{\partial\mathcal{L}_0}{\partial R} + \frac{\partial\mathcal{L}_p}{\partial R} = 0 \quad (\delta R). \quad (16)$$

On assuming that the vortex parameters are independent of the angular variable, we obtain the dispersion relation from the variational equations

$$\dot{\sigma} + \frac{1}{3w^2} - \frac{2}{3}\delta^{-1}a^2R^2 = 0 \quad (\delta a), \quad (17)$$

$$\dot{\sigma} - \frac{1}{3w^2} - \frac{1}{3}\delta^{-1}a^2R^2 = 0 \quad (\delta w). \quad (18)$$

Here the Peierls-Nabarro contributions are of small order as $R \to \infty$.

The variational equations (15) and (16) have fixed points which correspond to a static vortex with $V=0$ and the radius R given by the solution of

$$\frac{\partial\mathcal{L}_0}{\partial R} + \frac{\partial\mathcal{L}_p}{\partial R} = 0. \quad (19)$$

The variational equation (19) has to be solved coupled to the variational equations (17) and (18). The variational equations (17) and (18) give the dispersion relation for the vortex

$$a = \sqrt{\frac{3}{2}}\frac{\delta^{1/2}}{wR} \quad \text{and} \quad \dot{\sigma} = -\frac{1}{w^2}. \quad (20)$$

Using the variational equation (17) in the variational equation (19) gives

$$0 = \frac{\partial\mathcal{L}_0}{\partial R} + \frac{\partial\mathcal{L}_p}{\partial R} = \frac{16}{3}\delta^{-1}a^4wR^4 + \delta^{-1}a^4wR^{7/2} - \frac{32\pi^{7/2}}{3}\delta^{-1}a^4w^4R^{9/2}e^{-\pi^2 w}\sin(2\pi R - \pi/4). \quad (21)$$

Let us assume that w is $O(\delta^{1/2})$, so that $w=(\alpha\delta)^{1/2}$. Then using the results (20) in Eq. (21) gives the equation for the radius R as

$$1 - 2\pi^{7/2}(\alpha\delta)^{1/2}R^{1/2}e^{-\pi^2\sqrt{\alpha\delta}}\sin(2\pi R - \pi/4) = 0. \quad (22)$$

For large R this equation has the solution

$$\sin(2\pi R - \pi/4) = 0, \quad (23)$$

which results in

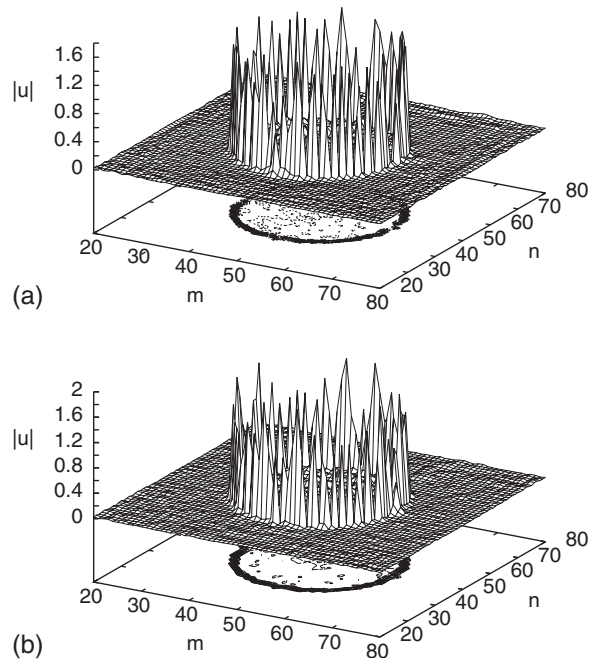

FIG. 1. Solution of DNLS equation (1) for vortex initial condition (4) with $a=0.1$, $w=0.3$, $V=0$, $R=15.5$, $g=0$, and $\delta=0.05$. (a) Solution at $t=30$; (b) perturbed solution with $a=0.1[1+0.2\cos(4\theta)]$ at $t=20$.

$$R=\frac{q\pi}{2}+\frac{1}{8} \tag{24}$$

at the fixed point, where q is a positive integer. The radii R_q are minima of the potential, provided that q is odd. For q even, the vortex will be unstable since it is located at a maximum of the Peierls-Nabarro potential. Hence the only stable vortices are for q odd.

For the parameter values of Fig. 1, Eq. (20) gives a vortex amplitude of $a=1.2$, which compares well with the average amplitude of the vortex in Fig. 1(a). However, it can be that the trial function does not include the circumferential oscillations seen in the numerical solution. Furthermore, from Eq. (22) it can be seen that as the DNLS equation becomes continuous in the limit of large δ the vortex becomes unstable. This is because for a given radius R, as δ increases, the stable and unstable roots of (22) coalesce, losing the vortex. For the parameter values of Fig. 1, Eq. (22) predicts that the vortex ceases to exist at $\delta=0.57$. Numerical results show that at $\delta=0.5$ the vortex structure begins to develop large gaps between the peaks and the vortex completely disappears at $\delta=0.689$. The modulation theory results are then in good quantitative agreement with the numerical results.

The solution (20) and (24) gives a family of vortices parametrized by their radius and their width. In the continuum limit these vortices will be unstable to azimuthal perturbations in w, with angular wave number $\ell=2$ being the fastest growing mode [18]. It will now be shown how discreteness, as captured by the Peierls-Nabarro potential in Eqs. (21) and (22), stabilizes the vortex.

To study the stability of the discrete vortex, we proceed as in Minzoni *et al.* [18] and expand the averaged Lagrangian about the fixed point to quadratic order, taking $w=w_q+\tilde{w}$, which results in

$$\mathcal{L}_f=\int_{t_0}^{t_1}\left(2awR^2\tilde{w}\dot{g}-\frac{IRa^2}{w}\tilde{w}_\theta^2-\frac{2\Lambda_1}{R}g_\theta^2-4\Lambda_1R^3\dot{\sigma}g^2+4\delta^{-1}a^2wR^5g^2-\frac{\tilde{w}^2}{2}H_{ww}(R_q,w_q)\right)dt. \tag{25}$$

Here Λ_1 is a function of R which will be determined in the analysis. The Hamiltonian equations derived from the Lagrangian (25) will have oscillatory solutions, provided that the corresponding quadratic form is positive definite. Otherwise the linearized equations show that the discrete vortex is unstable. For $w=O(\delta)$ and R_q at a minimum of the Peierls-Nabarro potential, $H_{ww}(R_q,w_q)>0$. In this case the corresponding quadratic form has to be studied in detail in order to determine the stability of the vortex.

The Euler-Lagrange equations for the linearized averaged Lagrangian (25) are

$$\dot{g}=-\frac{2IRa^2}{w}\tilde{w}_{\theta\theta}-H_{ww}\tilde{w},$$

$$\dot{w}=\frac{2\Lambda_1}{R}g_{\theta\theta}-(2\Lambda_1R^3\dot{\sigma}-4\delta^{-1}R^5a^2w)g, \tag{26}$$

where the time is rescaled with $2awR^2$. The solutions of these linearized modulation equations are readily obtained in terms of the normal modes,

$$\begin{pmatrix}g\\w\end{pmatrix}=e^{\lambda t}e^{i\ell\theta}\begin{pmatrix}G\\W\end{pmatrix}, \tag{27}$$

where G and W are constants. The equation for the eigenvalue λ is

$$\lambda^2+\left(\frac{2Ia^2}{Rw}\ell^2-H_{ww}\right)\left(\frac{2\Lambda_1}{R}\ell^2-(4\delta^{-1}R^5a^2w-2\Lambda_1R^3\dot{\sigma})\right)=0. \tag{28}$$

In this eigenvalue equation, one root $\lambda_2<0$ for small and large ℓ, but is positive when

$$\frac{Rw}{Ia^2}H_{ww}\leqslant\ell^2\leqslant\frac{R}{2\Lambda_1}(4\delta^{-1}R^5a^2w-2\Lambda_1\dot{\sigma}). \tag{29}$$

To determine the stability of the vortex, the width of the shelf needs to be determined, so that Λ_1 can be calculated.

In an unstable region, if present, the vortex should have small but finite amplitude deformations. This possibility was explored by taking Λ_1 as a bifurcation parameter to produce the desired deformation waves. The solutions of the nonlinear equations arising from (26) on keeping higher-order terms do not have periodic solutions of period 2π. We therefore conclude that there is no instability region. To finish the stability analysis, we need to find Λ_1 which satisfies

$$4R^5a^2w-2\Lambda_1\dot{\sigma}=\frac{Rw}{Ia^2}H_{ww}. \tag{30}$$

This gives $\Lambda_1=w+wH_{ww}/(Ia^2R^{7/2})$. The mode

$$\ell^2 = \frac{Rw}{Ia^2} H_{ww} \tag{31}$$

then has zero growth rate, which implies marginal stability. This marginal mode is interpreted as an approximation to a very long-period perturbation. Substituting values for Λ_1 and $\dot{\sigma}$ gives $\ell=4$ as a long-lifetime mode. Using the numerical values in Fig. 1 the critical mode wave number is obtained from Eq. (31) as 4.382…, which is a good approximation to the actual value of 4. To test this conclusion the steady vortex was perturbed with an amplitude $a_p(\theta)=a(1+\epsilon\cos 4\theta)$, which is a wave with $\ell=4$. The results are shown in Fig. 1(b). On comparing this figure with Fig. 1(a) the effect of this long-lifetime mode can be seen, as the perturbation in amplitude has resulted in an increase in amplitude of the azimuthal wave around the vortex. Amplitude perturbations with modes either side of $\ell=4$ result in smaller-amplitude perturbations of the azimuthal wave.

IV. THIN RECTANGULAR VORTICES

It has been shown that the Peierls-Nabarro potential is responsible for the stability of a discrete vortex due to the trapping of the vortex maximum by the corresponding potential. It is then expected that the same mechanism will be able to sustain stable structures of various shapes, when δ is sufficiently small.

As a first, simple example let us consider a periodic solution concentrated along a straight line. The approximate trial function is

$$u_{mn} = \begin{cases} a(\operatorname{sech}\psi)e^{i\tau} + ige^{i\sigma t} & \text{for } x_2(t) \leqslant m \leqslant x_1(t), \\ 0 & \text{otherwise,} \end{cases}$$

$$\psi = \frac{n - y(t)}{w},$$

$$\tau = \sigma t + \theta_{mn} + (m - x_1)V_x^{(1)} + (m - x_2)V_x^{(2)} + [n - y(t)]V_y. \tag{32}$$

We choose the phase θ_{mn} to obtain a phase τ which behaves as $(m-x_1)V_x^{(1)}$ for $x_1 < m \leqslant x_1+\rho$, $(m-x_2)V_x^{(2)}$ for $x_2-\rho \leqslant m \leqslant x_2$, and constant in the region $x_1+\rho \leqslant m \leqslant x_2-\rho$. In this approximation the end points move independently. The shelf g is concentrated about $y(t)$, which is the position of the maximum of the vortex. The end points x_1 and x_2 of the line segment are allowed to evolve as functions of time t. Numerical solutions show that the line vortex develops a modulated mean level due to an undular bore propagating in from the ends (see Fig. 2). To account for this the amplitude a is modified to become $a(1+\mu(x/x_1)^2)$ to include the depression produced by the waves entering the vortex from its edges. For this special case of a symmetric trial function the averaged Lagrangian is

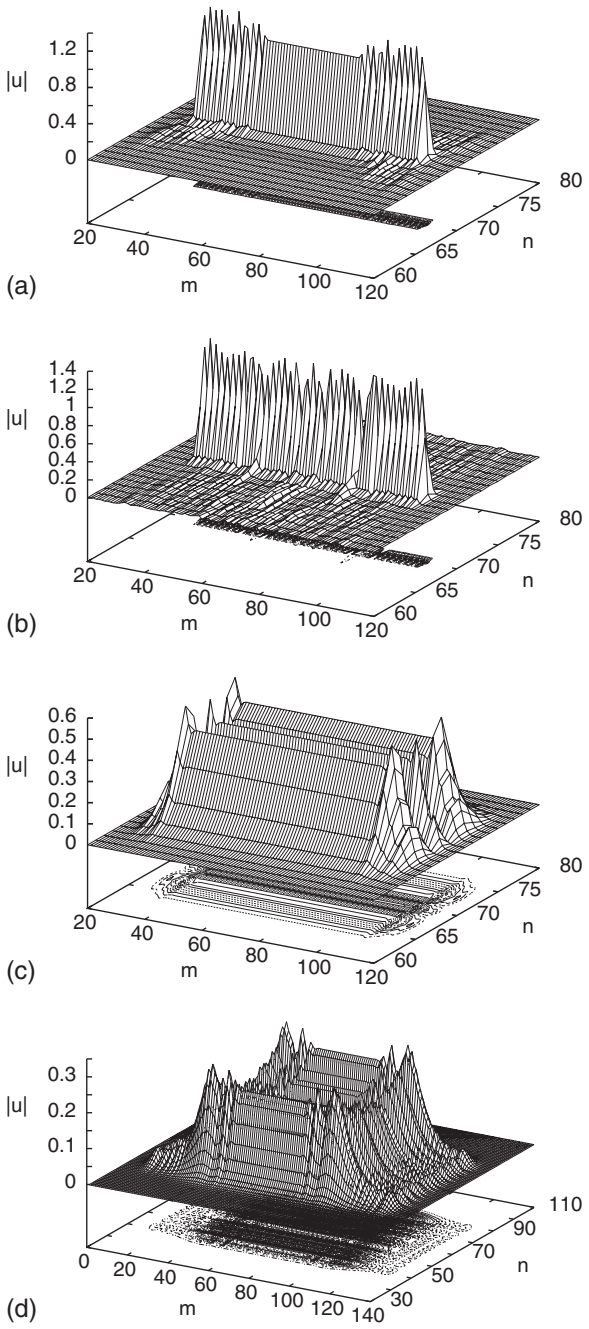

FIG. 2. Solution of DNLS equation (1) for wall initial condition (32) with $a=1.0$, $w=0.3$, $g=0$. Solution at (a) $t=3$ for $\delta=0.05$, (b) $t=30$ for $\delta=0.05$, (c) $t=2$ for $\delta=5$, and (d) $t=10$ for $\delta=5$.

$$\mathcal{L} = 2a^2 w x_1 \left(\sigma + \rho \dot{x}_1 V_x^{(1)} - \frac{1}{2}\rho V_x^{(1)2} + \dot{\zeta} V_y - \frac{1}{2} V_y^2 \right) - \frac{4}{3} x_1 \left(\frac{a^2}{w} + 2\delta^{-1} a^4 w \right) - \frac{8}{3x_1} \mu^2 a^2 w. \tag{33}$$

The contribution of the Peierls-Nabarro potential takes the form

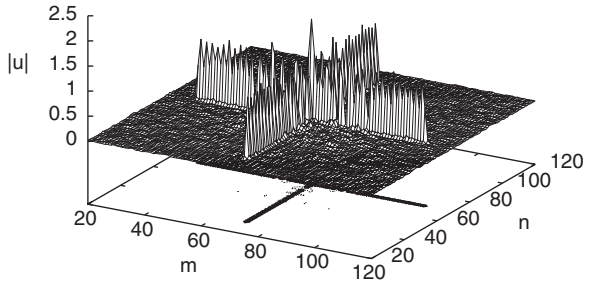

FIG. 3. Solution of DNLS equation (1) for cross initial condition at $t=30$.

$$\mathcal{L}_p = \frac{3}{\pi\delta}a^4 w \cos 2\pi x_1. \tag{34}$$

It is to be noted that unlike the Peierls-Nabarro contribution for a circular vortex (13), the Peierls-Nabarro potential for this line vortex is generated by the ends of the vortex. Therefore as δ increases it is only algebraically small in δ since $w \sim \delta^{1/2}$.

As before, for δ sufficiently small, the equations of motion derived from this averaged Lagrangian show trapping of the straight line segment by the Peierls-Nabarro potential. The modulation equations for the steady-state line vortex are

$$\sigma + \frac{4}{3w^2} + \frac{8}{3\delta}a^2 - \frac{8}{3}\frac{\mu^2}{x_1^2} + 6\delta^{-1}a^2 w \sin 2\pi x_1 = 0, \quad \delta x_1,$$

$$\sigma - \frac{4}{3w^2} - \frac{8}{3\delta}a^2 - \frac{8}{3x_1^2}\mu^2 a = 0, \quad \delta w,$$

$$\sigma + \frac{4}{3w^2} - \frac{16}{3\delta}a^2 - \frac{8}{3x_1^2}\mu^2 a = 0, \quad \delta a. \tag{35}$$

Since we are interested in large vortices, we have to leading order that

$$\sigma = -\frac{4}{3w^2} - \frac{8}{3\delta}a^2, \tag{36}$$

with a dispersion relation similar to that for the circular vortex

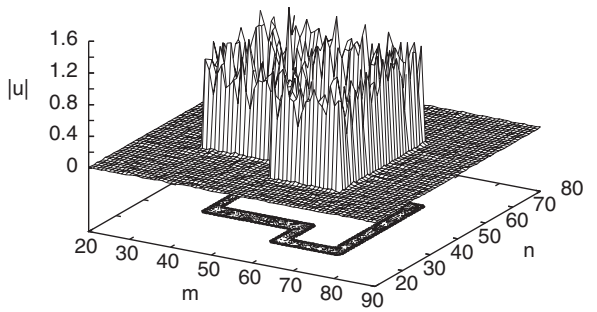

FIG. 4. Solution of DNLS equation (1) for the L-shaped initial condition at $t=30$.

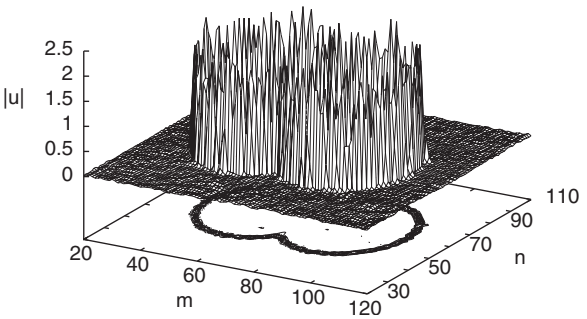

FIG. 5. Solution of DNLS equation (1) for figure of 8 initial condition at $t=30$.

$$\delta^{-1}a^2 w^2 = \frac{1}{4}. \tag{37}$$

The higher-order terms in the δx_1 equation in the modulation equations (35) give the size of the vortex as the solution of

$$\frac{\mu^2}{x_1^2} = \frac{9}{2}\delta^{-1}a^2 w \sin 2\pi x_1. \tag{38}$$

This solution shows that as δ increases the solutions x_1 become larger. A line vortex of a given size then destabilizes as δ increases due to the coalescence of a stable and an unstable solution. This situation is analogous to that for the circular vortex.

The modulation equations for the shelf g and the width perturbation $\tilde{w}$ can be developed in a similar manner as for the circular vortex. However, these equations will not be analyzed as the main stability result does not come from the oscillations in the body of the vortex, but from the end points. This stability mechanism is described above.

The initial evolution of the line vortex is shown in Fig. 2(a) in which the waves generated at the ends of the vortex are seen to propagate into the vortex, in the manner of an undular bore. In the modulation equations μ cannot be determined variationally as the form of a suitable, simple trial function which captures the end point behavior is not clear. As δ increases it follows from the modulation equation (38)

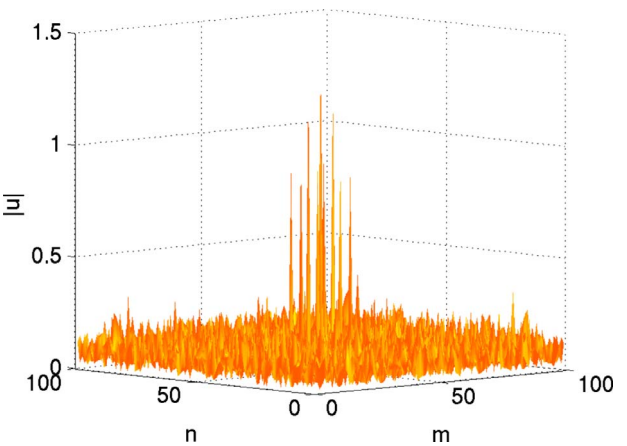

FIG. 6. (Color online) 12-peak solution of DNLS equation, $\delta = -0.1$.

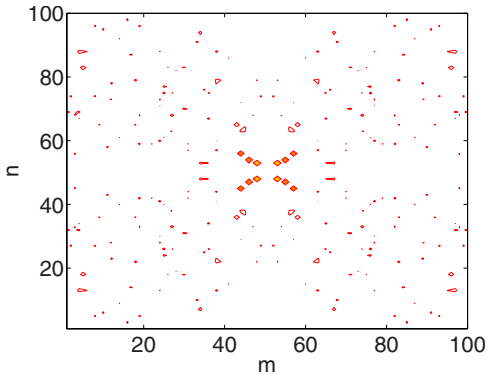

FIG. 7. (Color online) Contour plot of 12-peak solution of DNLS equation, $\delta=-0.1$.

that the Peierls-Nabarro potential can no longer hold the vortex, as can be seen in Fig. 2(c). It can also be seen that an undular bore develops at the leading and trailing edges of the vortex and expands into it. This bore expands the vortex, with it expanding symmetrically into $y>0$ and $y<0$, as required by momentum conservation.

This same mechanism operates for more complicated structures, such as the cross shown in Fig. 3. Here the two arms of the cross act independently and can sustain a stable structure. This type of solution was also studied by MacKay and Aubry [9], who called them rivers. In the work of MacKay and Aubry continuation ideas were used, while in the present work a large-scale mechanism which stabilizes these structures is determined. This stabilization process is due to the trapping by their self-consistent Peierls-Nabarro potential.

V. POLYGONS AND OTHER SHAPES

Building on the thin rectangular vortex, we can construct vortices of arbitrary shape by adding straight line segments, parallel to the coordinate axes, to make a polygonal path. Clearly the phase will have to increase by 2π after a circuit of this polygonal vortex. Therefore, if the vortex has a total length D, it will be assumed that the phase increases at the uniform rate $\dot{\theta}=2\pi/D$ along the polygonal vortex. The same arguments used for the straight line vortices can be applied to each side of the vortex, each side acting as an independent structure. Again instability is observed for δ sufficiently large. As for the straight line vortex the instability initiates at the corners, which are the ends of the straight line segments. An example of such a segmented, stable vortex, which has an L shape, is shown in Fig. 4. This L shape was obtained from the evolution of an initial condition constructed with straight line vortices, with a phase which increases at a rate $\dot{\theta}=2\pi/D$, where D is the total length of the vortex.

Finally this same construction of complicated vortices from fundamental units can be used to construct the figure of 8 vortex shown in Fig. 5. This shape was obtained by evolving two circular vortices, as in Fig. 1, after deleting the inner portions. The phase again has a constant rate of increase around the vortex, for a total change of 2π.

It is clear that this construction of vortices or rivers with complicated shapes can be continued. Again these vortices will be stable for very discrete lattices, that is for $\delta \ll 1$, and as δ increases they will be become destabilized and so decay.

In addition to time periodic solutions, the two-dimensional DNLS equation appears to support a class of more general localized solutions that are an approximate superposition of breathers with different frequencies. For these solutions we have a set of active sites U, where for m,n for these active sites U we have $u_{mn}\sim C_{mn}e^{i\omega_{mn}t}$ with $C_n \sim 1\pm\delta$, otherwise $u_{mn}\sim O(\delta)$. The amplitudes C_{mn} and frequencies ω_{mn} for the active sites appear to vary slowly in time to within a small percentage of some average value that

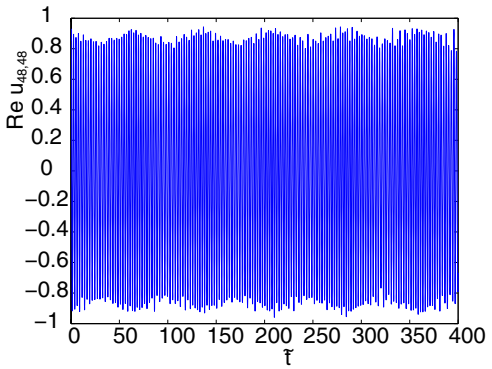

FIG. 8. (Color online) Re($u_{48,48}$) at sites of inner square as a function of time ($t=-\delta\tilde{t}$).

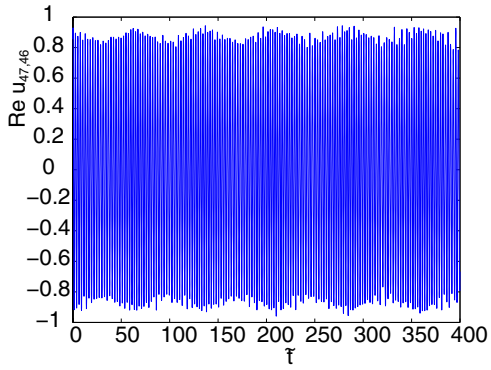

FIG. 9. (Color online) Re($u_{47,46}$) at sites of middle square as a function of time ($t=-\delta\tilde{t}$).

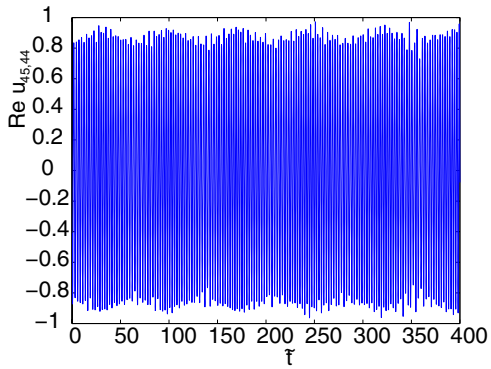

FIG. 10. (Color online) Re($u_{45,44}$) at sites of outer square as a function of time ($t=-\delta\tilde{t}$).

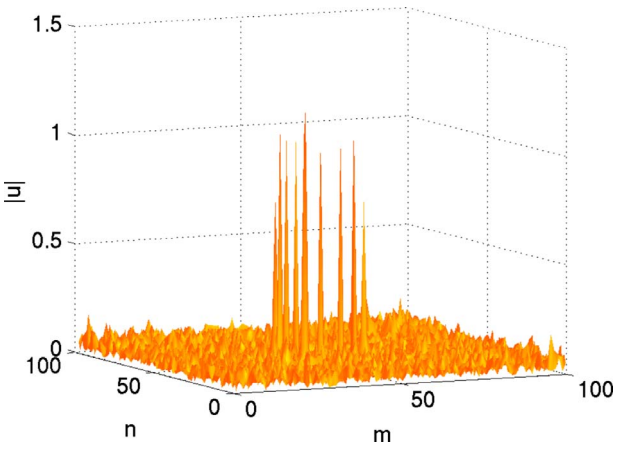

FIG. 11. (Color online) L-shaped solution of the DNLS equation, $\delta=-0.1$.

depends on the site. Unlike the case for breather (vortex) solutions, we observe that the ω_{mn} are not the same for all active sites.

An example can be seen in Fig. 6, where we have used periodic boundary conditions with $\delta=-0.1$. The peaks are seen clearly in the contour plot shown in Fig. 7. They are located at the three sets of sites

$$U_1 = \{(48,48),(53,48),(53,53),(48,53)\},$$

$$U_2 = \{(47,46),(54,46),(54,54),(47,55)\},$$

$$U_3 = \{(45,44),(56,44),(56,57),(44,57)\},$$

of a 100×100 lattice. Each U_j defines a parallelogram, with U_1 the "inner," U_2 the "middle," and U_3 the "outer" parallelogram. In Figs. 8–10 we show the real parts of u at the sites $(48,48)\in U_1$, $(47,46)\in U_2$, and $(45,44)\in U_3$. The values of u at all four sites in each U_j are seen to be identical to the corresponding three representative sites shown in the figures. We furthermore see that the (average) amplitudes for U_1, U_2, and U_3 are 1.25, 0.92, and 0.83, respectively. The corresponding (average) periods for U_1, U_2, and U_3 are 1.60, 2.24, and 2.70. Comparing the amplitudes of the three U_j, we see some periodic energy interchange between the middle

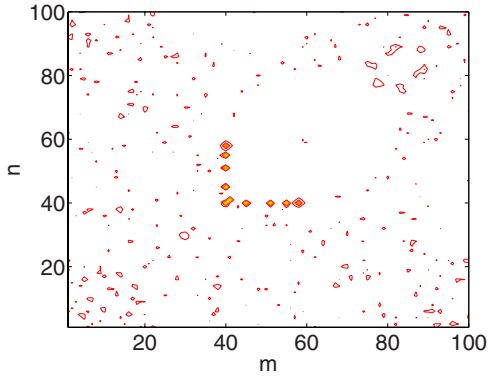

FIG. 12. (Color online) Contour plot of L-shaped solution of the DNLS equation, $\delta=-0.1$.

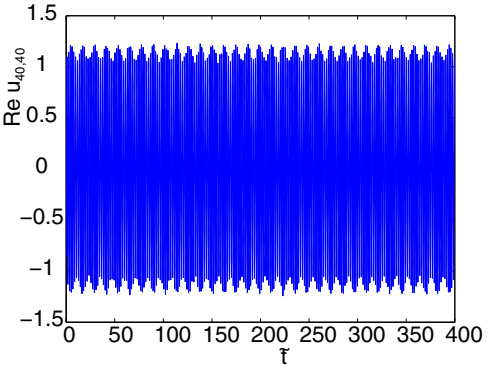

FIG. 13. (Color online) $\mathrm{Re}(u_{40,40})$ as a function of time ($t=-\delta\tilde{t}$).

and outer parallelograms. The different average frequencies in each parallelogram imply that these solutions are not breathers, but rather an approximate superposition of three slightly modulated breather solutions. Similar solutions are seen for periodic and free boundary conditions on the finite lattice. In both cases the localized solutions appear to be stable in that we do not see any tendency for the amplitudes of the main peaks to diminish. Adding a small boundary damping with $\nu\leqslant 10^{-2}$ as in [5] does not alter the amplitudes of the peaks over several hundreds of periods.

A second example is seen in Fig. 11, with the corresponding contour plot shown in Fig. 12. The L-shaped pattern of peaks consists of the corner sites (40,40) and (41,41) and the four pairs of sites $U_1=\{(40,45),(45,40)\}$, $U_2=\{(40,51),(51,40)\}$, $U_3=\{(40,55),(55,40)\}$, and $U_4=\{(40,58),(58,40)\}$. The motion of the two sites in each U_j is identical. In each site we see an oscillation with a slow modulation; see, e.g., Figs. 13 and 14 where we show the real part of u_{mn} at the sites $(m,n)=(40,40)$ and (58,40), respectively. The average frequencies at the different U_j are different, for example at (40,51), (40,55), and (40,55) we see the frequencies 1.80, 1.90, and 2.85, respectively. The L-shaped pattern is therefore not a breather, but rather an approximate superposition of six breathers peaked at (40,40), (41,41), and the four U_j. There is also evidence of some energy interchange between the peaks at (40,40) and (41,41). As for the first example, similar solutions are observed for both periodic and free boundary conditions and the peaks persist under small boundary damping.

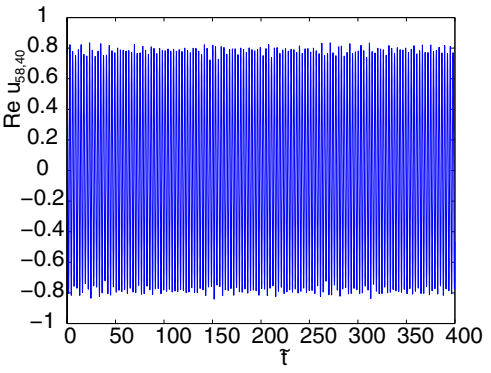

FIG. 14. (Color online) $\mathrm{Re}(u_{58,40})$ as a function of time ($t=-\delta\tilde{t}$).

VI. CONCLUSIONS

It has been shown that discrete lattices can sustain stable, periodic vortices of arbitrary shape with a linearly increasing phase. A modulation theory was developed which explained the stability of these vortices. In particular this modulation theory included the Peierls-Nabarro potential generated by the continuum vortices and was found to be responsible for the stability for δ sufficiently small. The approximate solutions of this modulation theory show how the discreteness of the lattice stops the breakup of the vortices. This mechanism is very different from that which stabilizes vortices in nematic liquid crystals, as in this continuous medium nonlocality decreases the destabilization terms [18]. For the present discrete media the Peierls-Nabarro potential stabilizes the discrete vortices. This Peierls-Nabarro potential is absent in continuous media.

For the case of straight line vortices it was found that the finite size of the vortex produces waves which travel from its edges toward its center, producing a modulated mean level whose length scale is the length scale of the vortex. This mean level change produces the Peierls-Nabarro potential which traps the vortex.

In general, the vortices are sustained by the Peierls-Nabarro potential, which traps them at a minimum, with the same potential preventing their breakup. On the other hand, as the lattice approaches the continuum limit, the potential is no longer sufficient to trap them, so that they collapse.

It should be remarked that the present modulation theory approach gives accurate predictions in simple terms for both the qualitative and quantitative features of the evolution.

A further feature of some of the localized solutions examined here is a temporal behavior that is unlike that of the well-known breather solutions. Such localized solutions may correspond to exact solutions of the infinite lattice, or to slowly decaying states that may be close to exact solutions for finite lattices. Possible subtle differences between the stable localized states in finite and infinite lattices can be due to slow decay due to radiation in the infinite case [16]. These differences may be difficult to capture numerically, but may give distinct long-time predictions for optical vs molecular or condensed matter systems modeled more realistically by the DNLS equation on finite and infinite lattices, respectively.

Similar ideas to those developed here could be used for the study of other types of vortices, such as nonlocal discrete vortices. This is the subject of ongoing studies.

ACKNOWLEDGMENTS

The authors would like to thank Professor Yuri Kivshar for discussions about and insights into the work presented in this paper. This research was supported by the Engineering and Physical Sciences Research Council (EPSRC) under Grant No. EP/D075947/1 and by CONACyT under Grant No. 50303.

[1] D. N. Christodoulides and R. I. Joseph, Opt. Lett. **13**, 794 (1988).
[2] A. B. Aceves, C. de Angelis, T. Peschel, R. Muschall, F. Lederer, S. Trillo, and S. Wabnitz, Phys. Rev. E **53**, 1172 (1996).
[3] R. Morandotti, U. Peschel, J. S. Aitchison, H. S. Eisenberg, and Y. Silberberg, Phys. Rev. Lett. **83**, 2726 (1999).
[4] D. N. Christodoulides, F. Lederer, and Y. Silberberg, Nature (London) **424** 817 (2003).
[5] R. Livi, R. Franzosi, and G. L. Oppo, Phys. Rev. Lett. **97**, 060401 (2006).
[6] G. Kopidakis, S. Aubry, and G. P. Tsironis, Phys. Rev. Lett. **87**, 165501 (2001).
[7] S. Aubry, Physica D **216**, 1 (2006).
[8] A. J. Sievers and S. Takeno, Phys. Rev. Lett. **61**, 970 (1988).
[9] R. S. MacKay and S. Aubry, Nonlinearity **7**, 1623 (1994).
[10] M. I. Weinstein, Nonlinearity **12**, 673 (1999).
[11] J. M. Bergamin, T. Bountis, and C. Jung, J. Phys. A **33**, 8059 (2000).
[12] D. E. Pelinovsky, P. G. Kevrekidis, and D. J. Frantzeskakis, Physica D **212**, 20 (2005).
[13] M. J. Ablowitz and Z. H. Musslimani, Phys. Rev. Lett. **87**, 254102 (2001).
[14] A. Fratalocchi and G. Assanto, Phys. Rev. E **72**, 066608 (2005).
[15] R. Carretero-Gonzáles, J. D. Talley, C. Chong, and B. A. Malomed, Physica D **216**, 77 (2006).
[16] D. Bambusi and D. Vella, Discrete Contin. Dyn. Syst., Ser. B **2**, 389 (2002).
[17] G. B. Whitham, *Linear and Nonlinear Waves* (John Wiley and Sons, New York 1978).
[18] A. A. Minzoni, N. F. Smyth, A. L. Worthy, and Y. S. Kivshar, Phys. Rev. A **76**, 063803 (2007).
[19] L. A. Cisneros and A. A. Minzoni, Physica D (to be published).